Asymmetric chromosome segregation and cell division in DNA damage-induced bacterial filaments

Suchitha Raghunathan[a,b], Afroze Chimthanawala[a,c], Sandeep Krishna[a,d], Anthony G. Vecchiarelli[e], and Anjana Badrinarayanan[a,*]

[a]National Centre for Biological Sciences, Tata Institute of Fundamental Research and [d]Simons Centre for the Study of Living Machines, Bangalore 560065, India; [b]The University of Trans-Disciplinary Health Sciences and Technology (TDU), Bangalore 560064, India; [c]SASTRA University, Thanjavur, Tamil Nadu 613401, India; [e]Molecular, Cellular, and Developmental Biology Department, Biological Sciences Building, University of Michigan, Ann Arbor, Michigan 48109

ABSTRACT **Faithful propagation of life requires coordination of DNA replication and segregation with cell growth and division. In bacteria, this results in cell size homeostasis and periodicity in replication and division. The situation is perturbed under stress such as DNA damage, which induces filamentation as cell cycle progression is blocked to allow for repair. Mechanisms that release this morphological state for reentry into wild-type growth are unclear. Here we show that damage-induced *Escherichia coli* filaments divide asymmetrically, producing short daughter cells that tend to be devoid of damage and have wild-type size and growth dynamics. The Min-system primarily determines division site location in the filament, with additional regulation of division completion by chromosome segregation. Collectively, we propose that coordination between chromosome (and specifically *terminus)* segregation and cell division may result in asymmetric division in damage-induced filaments and facilitate recovery from a stressed state.**

Monitoring Editor
Erin Goley
Johns Hopkins University

Received: Aug 21, 2020
Revised: Oct 23, 2020
Accepted: Oct 23, 2020

INTRODUCTION

For successful cell division to occur, accurate DNA duplication and segregation must be completed. In bacteria, chromosome replication initiates bidirectionally from an "*origin*" and finishes opposite to this position, at the "*terminus*" (Kleckner *et al.*, 2014, 2018; Reyes-Lamothe and Sherratt, 2019). Several factors ensure that cells divide only upon completion of this process by regulating the multiprotein division machinery called the "divisome" (Galli and Gerdes, 2012; Männik *et al.*, 2016; Dewachter *et al.*, 2018; Kleckner *et al.*, 2018). For example, *Escherichia coli* encode negative regulators of the tubulin homologue FtsZ that is required to initiate the assembly of the divisome at the division plane. Nucleoid occlusion by SlmA prevents the formation of the FtsZ-ring at locations where chromosomal DNA is present and MinCDE oscillations direct the position of the Z-ring near midcell (Bernhardt and de Boer, 2005; Tonthat *et al.*, 2011; Tsang and Bernhardt, 2015). Recent studies have also suggested coordination of division with the *terminus* via proteins such as MatP and ZapAB that act as a bridge between the DNA as well as the divisome (Mercier *et al.*, 2008; Espéli *et al.*, 2012; Männik *et al.*, 2016). Together, in unperturbed laboratory conditions, this results in daughter cells that replicate and divide in a periodic manner and that do not show much deviation in birth and division cell sizes (Donachie, 1968; Campos *et al.*, 2014; Taheri-Araghi *et al.*, 2015; Harris and Theriot, 2016; Wallden *et al.*, 2016; Micali *et al.*, 2018; Si *et al.*, 2019). Such size maintenance has been described in other bacteria as well as eukaryotic systems (Soifer *et al.*, 2016; Chandler-Brown *et al.*, 2017; Lambert *et al.*, 2018).

This article was published online ahead of print in MBoC in Press (http://www.molbiolcell.org/cgi/doi/10.1091/mbc.E20-08-0547) on October 28, 2020.

The authors declare no competing interests.

Author contributions: S.R. conceptualized the project, designed the experiments, executed the experiments, analyzed the data, and wrote the manuscript. A.C. designed the experiment, executed the experiments, and analyzed the data related to RecA. S.K. analyzed and interpreted the data, and wrote the manuscript. A.V. prepared the reagents and tools, and interpreted the data. A.B. conceptualized the project, designed the experiments, wrote the manuscript, and acquired funding.

*Address correspondence to: Anjana Badrinarayanan (anjana@ncbs.res.in).

Abbreviations used: IPTG, Isopropyl β-D-1-thiogalactopyranoside; LB, Luria Broth; LD, long daughter; M9-Cas, M9–casamino acids; MMC, mitomycin–C; NA, numerical aperture; OD600, optical density at 600 nm wavelength of light; SD, short daughter.

Recent investigations in bacteria have proposed that cells follow an "adder"-based principle, where length added between divisions is independent of the birth length of the cell. Size homeostasis is governed either via regulation at the stage of replication initiation or cell division or both (Campos *et al.*, 2014; Taheri-Araghi *et al.*, 2015; Wallden *et al.*, 2016; Si *et al.*, 2019). In addition, some studies have also proposed a role for cell shape or concurrency between processes of replication and division in size control (Harris and Theriot, 2018; Micali *et al.*, 2018). This homeostatic state is perturbed under conditions of stress, a situation that can be often faced by bacterial cells in their environment (Justice *et al.*, 2008; Horvath *et al.*, 2011; Yang *et al.*, 2016; Heinrich *et al.*, 2019). For example, under DNA damage, a cell cycle checkpoint blocks cell division until damage has been repaired. The bacterial SOS response is activated upon the binding of RecA to single-stranded DNA that is exposed as a consequence of DNA damage (Mukherjee *et al.*, 1998; Kreuzer, 2013; Jonas, 2014). As part of this response, a cell division inhibitor (such as SulA in *E. coli*) blocks polymerization of FtsZ, resulting in cellular elongation or filamentation (Mukherjee *et al.*, 1998; Kreuzer, 2013). Cell division inhibition during damage is a conserved process, even though the effectors may vary across bacteria. SOS-induced division inhibition is carried out by SidA in *Caulobacter* and YneA in *Bacillus* (Mukherjee *et al.*, 1998; Mo and Burkholder, 2010; Modell *et al.*, 2011; Jonas, 2014). SOS-independent DNA damage-induced division inhibitors have also been identified, suggesting that this is an important step in DNA repair (Modell *et al.*, 2014). Along with blocking division, chromosome cohesion is also initiated in these filaments. It is thought that this can aid recombination-based repair (Odsbu and Skarstad, 2014; Vickridge *et al.*, 2017).

Cells have also been shown to change shape and size under other forms of stress including host environments, heat shock, and osmotic fluctuations (Justice *et al.*, 2008; Bos *et al.*, 2015; Kysela *et al.*, 2016; Yang *et al.*, 2016; Caccamo and Brun, 2018; Wehrens *et al.*, 2018; Heinrich *et al.*, 2019). Together, this highlights the plasticity with which bacteria such as *E. coli* sample a range of cell sizes including filamentous and nonfilamentous cell lengths. The process by which cell division is regulated to result in elongation under DNA damage has been well characterized (Adler and Hardigree, 1965; Kantor and Deering, 1966; Suzuki *et al.*, 1967; Mukherjee *et al.*, 1998; Mo and Burkholder, 2010; Modell *et al.*, 2011, 2014; Jonas, 2014). Indeed, recent cell biological studies have also characterized division restoration dynamics of non-DNA damage-induced filaments (such as SulA overexpression or heat shock; Wehrens *et al.*, 2018). However, unlike these stresses, DNA damage specifically perturbs chromosome organization and segregation, with replication initiation continuing despite damage to DNA (Rudolph *et al.*, 2007; Lloyd and Rudolph, 2016). The impact of such a damage-induced state on reinitiation of wild-type-like division after repair is mechanistically less characterized.

In this study, we probe the mechanism by which filamentous *E. coli* reinitiate chromosome segregation and cell division after DNA repair. We use single-cell, time-resolved fluorescence microscopy to follow the kinetics of division restoration after cells face a pulse of DNA damage and observe that filamentous cells tend to divide asymmetrically, generating short daughters of wild-type size and growth dynamics. We further observe that division restoration is controlled by two steps: determining the *location* and *timing* of division. This process, regulated by a combination of MinCDE oscillations and chromosome (specifically *terminus*) segregation, is accompanied by asymmetric partitioning of repaired chromosomes, resulting in the production of daughter cells of wild-type size and devoid of DNA damage, thus likely facilitating recovery from a stressed state.

RESULTS

Asymmetric cell division in DNA damage-induced filaments

To understand how damage-induced filamentous *E. coli* reinitiate cell division and wild-type growth after DNA damage, we followed division restoration in cells after treatment with a subinhibitory dose of the DNA damaging agent mitomycin-C via time-lapse imaging (1 µg/ml; Dapa *et al.*, 2017; Figure 1A). While unperturbed wild-type cells divided near midcell (Figure 1B), we found that a significant proportion of cells deviated from this division pattern as they increased in length (Figure 1, C and D). Damage-treated cells close to wild-type length (5–10 µm) divided in the middle resulting in the production of two daughter cells of similar sizes. In contrast, filamentous cells divided asymmetrically to produce a short "daughter" cell (S_D) and a long cell that continued to filament (L_D; Figure 1, C and E). The probability of a cell to undergo asymmetric division increased with increasing cell length with 85% of cells dividing asymmetrically at lengths >12 µm. S_D production via asymmetric division was observed independent of growth media (Supplemental Figure S1A). In addition, as seen in the case of division-inhibited *E. coli* filaments (Wehrens *et al.*, 2018), cephalexin-treated cells (where division is inhibited, without perturbing genome integrity; Rolinson, 1980; Chung *et al.*, 2009) also tended to have increased non-midcell (asymmetric) divisions with increasing filament lengths (Supplemental Figure S1, B and C). Varying durations of damage exposure (30, 60, or 90 min) resulted in different degrees of filamentation. However, in each case, the S_D size distribution for these treatments was comparable. Additionally, >81% of S_D's were close to wild-type size distribution (Figure 1, F and G and Supplemental Figure S1, D–G). The frequency of non-midcell division was similar between filaments of comparable lengths (12–40 µm). However, the distribution of division site locations varied with varying cell length bins (discussed further in Figure 3 and the associated section, later in the article).

To characterize the recovery process further in DNA damage-induced filaments, we followed the fate of the filament (L_D) and the S_D over time. We observed that filamentous cells underwent multiple divisions in a 1 h time period, generating daughter cells (S_D) of wild-type size at each division (Figure 1I). In 16 ± 2% cases, the filament itself was restored to wild-type size during the course of imaging. In the same time, wild-type cells undergo three divisions on average, suggesting that more daughter cells are produced from a filament than a cell of the same size as wild type during recovery. In contrast to the filaments, daughter cells of wild-type size displayed growth and division dynamics similar to nondamage conditions (Figure 1, H and J). As an example, in Figure 1E, we followed the fate of an S_D (4.6 µm) generated from a filament and found that the daughter cell reinitiated wild-type growth dynamics soon after division. Time taken between divisions for S_D was close to the distribution seen for wild type, in contrast to interdivision times observed for the nonrecovered, filamentous L_D (Figure 1J). Consistently, the DNA damage marker, RecA, formed multiple foci in L_D at the time of division, while S_D had RecA localization as seen for wild-type cells (Lesterlin *et al.*, 2014; Rajendram *et al.*, 2015; Vickridge *et al.*, 2017) or elongated cells with no DNA damage (cephalexin treated; Supplemental Figure S1, K and J). Our observations are in line with the idea of the reversible nature of damage-induced filamentation (Rudolph *et al.*, 2007, 2010; Vickridge *et al.*, 2017) and suggest that filamentous cells can restore cell division and recover from a stressed state.

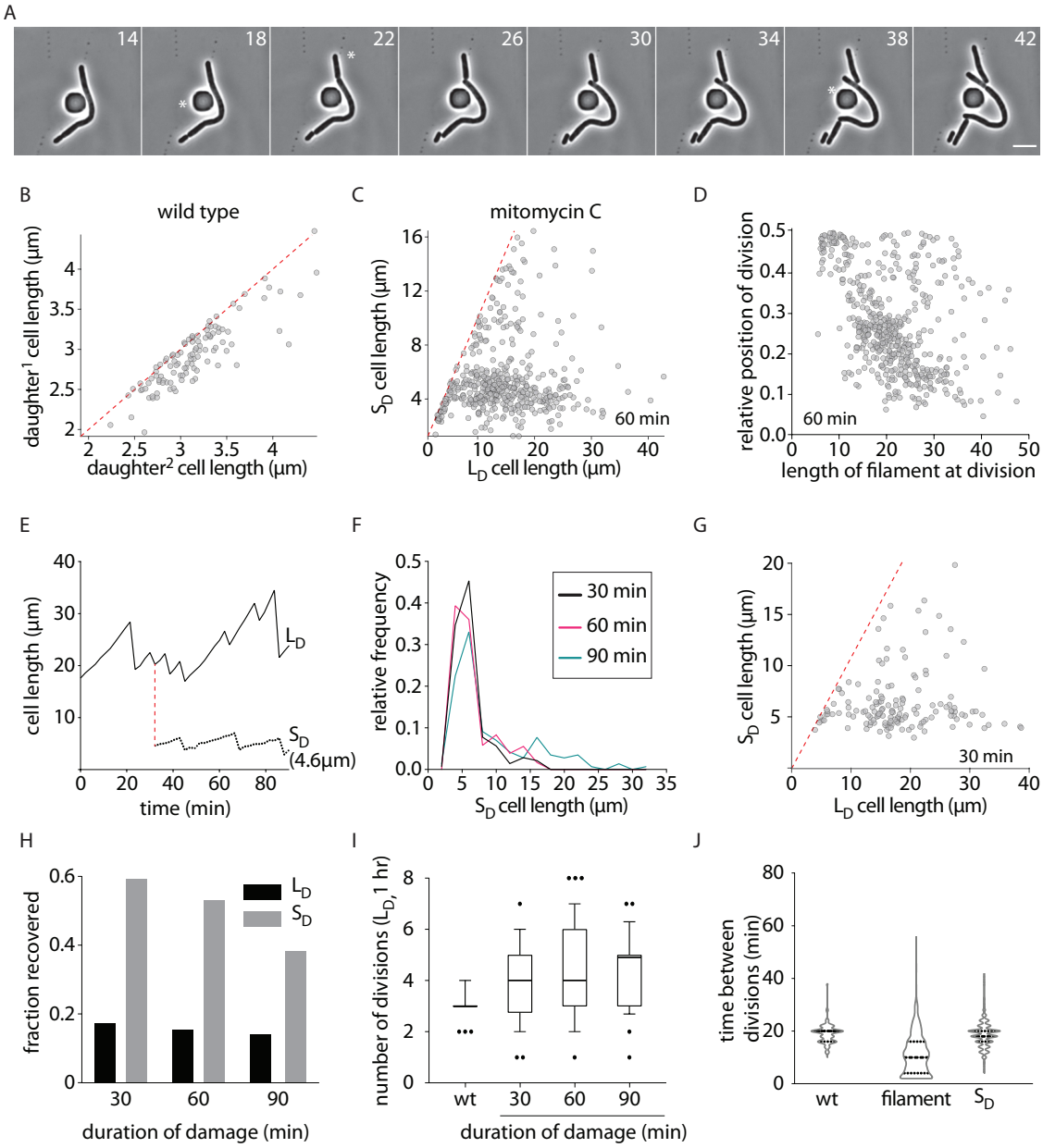

FIGURE 1: Asymmetric division in DNA damage-induced filaments during recovery. (A) Representative time-lapse montage of filamentous cells during recovery. White asterisks indicate divisions occurring toward a cell pole. Scale bar = 5 μm; time in minutes here and in all other images. Images were taken every 2 min. (B) Cell length of two daughter cells generated from a single division in wild-type conditions. Each gray dot represents a single division event ($n = 157$). The red line plots the expected values if all cells were dividing at their midpoint. (C) Cell length of long daughter (L_D) and short daughter (S_D) generated from a DNA damage-induced filament during recovery. Cells are treated with mitomycin-C (MMC) for 60 min. Each gray dot represents a single division event ($n = 531$). The red line plots the expected values if all cells were dividing at their midpoint. (D) Location of division is plotted as a function of cell length in filamentous *E. coli* during recovery from DNA damage treatment (60 min; $n = 531$). (E) Cell length of a long daughter (L_D) and short daughter (S_D) is tracked over time during damage recovery. Decrease in cell length is indicative of division. (F) Distribution of S_D lengths generated from filaments between 12 and 40 μm long after 30, 60, and 90 min of MMC treatment ($n = 142$ [30 min], 363 [60 min], 96 [90 min]). (G) As C for cells treated with MMC for 30 min ($n = 151$). (H) Fate of S_D and L_D during recovery. Cell is classified as recovered if it undergoes midcell division and produces a daughter of wild-type size and filamentous if it continues to filament after division ($n = 116$ [30 min, L_D], 98 [60 min, L_D], 106 [90 min, L_D], 150 [30 min, S_D], 264 [60 min, S_D], 150 [90 min, S_D]). (I) Number of divisions per cell in 1 h for all durations of damage treatment. As a control, the number of divisions wild-type cells undergo is also shown ($n = 50$ [wt], 150 [filaments]). (J) Distribution of time between divisions for wild-type (no damage control), damage-induced filament, and S_D during recovery from MMC ($n = 148$ [wt], 611 [filament], 468 [S_D]).

Consistently, we found that a viable cell count as well as cell length distribution was restored to close to that of wild type in the three treatment regimens within 120 min after recovery (Supplemental Figure S1, L and M). Taken together, our results are complementary to previous studies reporting non-midcell division events in filamentous *E. coli* (Begg and Doanachie, 1977; Taschner *et al.*, 1988; Rudolph *et al.*, 2009; Wehrens *et al.*, 2018). We thus characterized the factors contributing to S_D production in the case of damage-induced filaments.

Division dynamics of damage-induced filaments

In the case of wild-type steady-state population, where cells divide at midcell, the adder principle contributes to size homeostasis. Under adder, length added between divisions is thought to be independent of the length of the cell at birth (Campos *et al.*, 2014; Taheri-Araghi *et al.*, 2015; Wallden *et al.*, 2016; Si *et al.*, 2019). To understand what determines the distribution of short daughter sizes in the case of asymmetrically dividing damage-induced filaments, we further analyzed the growth and division dynamics of these filaments (details of cell division analysis are outlined in Figure 2, G and H, Supplemental Figure S2, D and E, and *Materials and Methods*). In damage-induced filaments, we found that length added between divisions did not correlate with length of the cell at birth. There were several instances of consecutive divisions without detectable elongation in between each division (Figure 2A). We also measured time between consecutive division events. While wild-type cells divided approximately every 20 min, filamentous cells displayed a large distribution of times. However, on average, longer cells tended to have shorter interdivision times, consistent with the observation that filamentous cells underwent an increased number of divisions when compared with wild type (Figure 2, B and C). In addition, we found that 67 ± 4% of divisions took place at the opposite pole of the previous division. This suggests that division did not preferentially occur only toward a single pole (old or new), with several instances of division events taking place in an alternating manner.

After damage, filament length increased at a characteristic rate, as seen in wild-type conditions (Supplemental Figure S2, A and B), with some fluctuation which probably arises because of stochasticity in damage and/repair. As stated above and expected for the adder principle seen in wild-type conditions, we found that length added between divisions had no correlation with birth length of filaments as well (Figure 2A). However, we noticed the following deviations from wild-type growth and division patterns in the case of damage-induced filaments: the distribution of added lengths was much broader than those seen for wild type; for example, 15% of divisions occurred without the addition of length between division events. When we assessed S_D length as a function of birth length of the filament, we found that there was some correlation between the two. Indeed, the extent of correlation was lesser when compared with steady-state growth, where the length of the daughter is strongly correlated with the birth length of the cell (Figure 2, D and F). To understand whether length added could explain the S_D size distribution we observed in the case of asymmetric division in filaments, we analyzed the distributions of length added and S_D length at each cell division (Figure 2E). We found that these distributions were significantly different, with length added having a broader distribution when compared with S_D sizes. Thus, based on previous studies (Wehrens *et al.*, 2018) and our current observations, this suggested to us that S_D size may be more strongly determined by spatial regulation of division events in the filament.

Role of Min-system in division positioning

To characterize the factors contributing to S_D production, we first assessed the localization of FtsZ in damage-induced filaments. We observed that the position of FtsZ shifted away from midcell as cell length increased and division occurred one-site-at-a-time in filaments during recovery (Figure 3A and Supplemental Figure S3A). In addition, the number of FtsZ rings did not scale significantly with increasing cell length, with most cells carrying only a single FtsZ-ring and very rarely two (Supplemental Figure S3A, bottom panel). Divisions were completed only one-site-at-a-time even in cephalexin-induced filaments, where 30% cells had more than one visible constriction site (Supplemental Figures S2D and S3D). Consistent with Wehrens *et al.* (2018), we also observed multiple Min localizations in filaments. Cells had one to two localizations at lengths between 5 and10 μm and this number increased with increasing cell length (Supplemental Figure S3B).

Furthermore, transcript levels of the divisome components did not appear to be perturbed in damage-induced filaments (Supplemental Figure S3C). We hence asked whether factors involved in division regulation contributed in wild-type conditions to S_D production during filamentous divisions. For this we assessed the effects of the loss of 1) nucleoid occlusion factor, SlmA, 2) negative regulator of FtsZ polymerization, SulA, and 3) the MinCDE system (de Boer *et al.*, 1989; Mukherjee *et al.*, 1998; Bernhardt and de Boer, 2005; Tonthat *et al.*, 2011; Kreuzer, 2013; Wehrens *et al.*, 2018). We found that deletion of *slmA* or *sulA* did not result in an increase in the number of constrictions in filaments (Supplemental Figure S3D). Furthermore, S_D size was comparable to that seen in wild-type filaments (Figure 3, B and C), suggesting that these factors may not contribute to division regulation in recovering filaments. In contrast, deletion of the *min* operon resulted in a more heterogeneous distribution of division site location when compared with wild type. Subsequently, distribution of S_D sizes was also found to be more heterogeneous with an increase in frequency of both minicells as well as divisions that could occur near midcell (Figure 3D and Supplemental Figure S3, E and F).

Our observations with *min*-deleted cells are consistent with previous studies implicating a role for Min-dependent division site regulation in filamentous *E. coli*. In Wehrens *et al.* (2018), a Min-dependent division site rule was established for filaments. According to this, there are multiple possible locations of division determined by the multiple nodes of the Min oscillation that vary based on length of the filament, with an equal possibility of division at each position. Given that we observed an effect of *min* deletion on S_D size determination, we asked whether this Min-rule could be recapitulated in the case of damage-induced filaments as well. We plotted the relative position of division for all three durations of DNA damage, binned in three size windows (12–18, 18–26, and 26–33 μm; based on analysis from Wehrens *et al.*, 2018; Figure 3, E–J). Consistent with the Min-rule, we found that filaments of length 12–18 μm showed high frequency of division near the ¼ position. However, in longer filaments (18–33 μm), divisions tended to occur at a higher frequency at the most polar site determined by this Min-rule, with low frequency of midcell division even at filament lengths where such division should be permitted (such as in the size range of 18–26 μm). Interestingly, at filament lengths between 33 and 40 μm, division position seemed more noisy. While division still tended to occur at a high frequency at the most polar division site (0.1–0.15), other sites also had a significant number of division events (e.g., 0.25–0.35). Indeed, this second site is close to the predicted location for possible divisions according to Min-driven division positioning. At these lengths midcell division also occurred; for

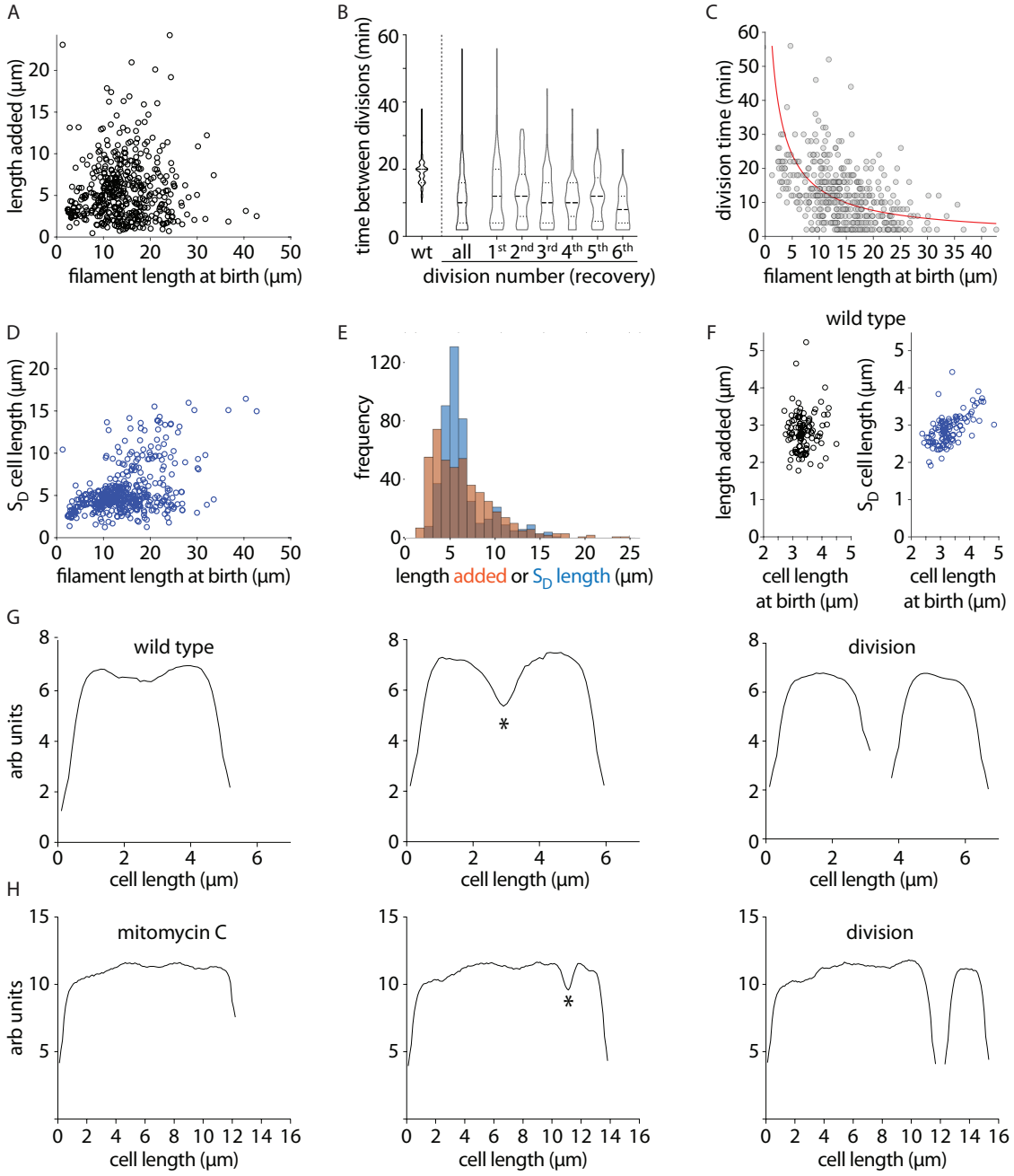

FIGURE 2: Division dynamics of damage-induced filaments. (A) Length added to a cell between divisions as a function of the birth length of the cell for MMC-treated cells ($n = 452$), p value 0.0293, 95% CI [–0.0631 0.1212], Pearson correlation value via MATLAB corrcoef function. (B) Time between divisions for wild-type cells or damage-recovery filaments for all divisions and for cells between first and second, second and third, and so on until the sixth division in filaments during recovery is plotted ($n = 148$ [wt], 410 [all filaments]). (C) Time between divisions as a function of cell length at birth for MMC-treated cells. Red line shows the relation that would be necessary for the system to be an adder (Eq. 3 in supplementary results), given that cells are growing exponentially with the rates given in Supplemental Figure S2A ($n = 458$). (D) S_D cell length as a function of the birth length of the cell for MMC-treated cells ($n = 457$, p value 0.4650, 95%CI [0.3894 0.5343], Pearson correlation value via MATLAB corrcoef function). (E) Distribution of length added and S_D cell length at each division for MMC-treated cells (distributions are significantly different, two-sample Kolmogorov-Smirnov test, p value 1.0721×10^{-8}, $n = 452$). (F) As A and D for wild-type cells (length added, $n = 107$, p value 0.0647, 95%CI [–0.1268 0.2514]; length removed, $n = 107$, p value 0.6057, CI [0.4698 0.7135], Pearson correlation value via MATLAB corrcoef function). (G) Phase profile for a wild-type cell before and after division is plotted. Constriction is marked with an * and divisions are identified during segmentation. (H) As G for a MMC-treated filament.

example, in 15% of filaments in the case of 90 min of damage treatment. Division patterns appear less clearly at longer lengths; however, the number of such long filaments is low across durations of damage. Such long filaments may have accumulated excessive DNA damage due to which recovery dynamics may also be compromised. Indeed, in general, division position seems less precise even

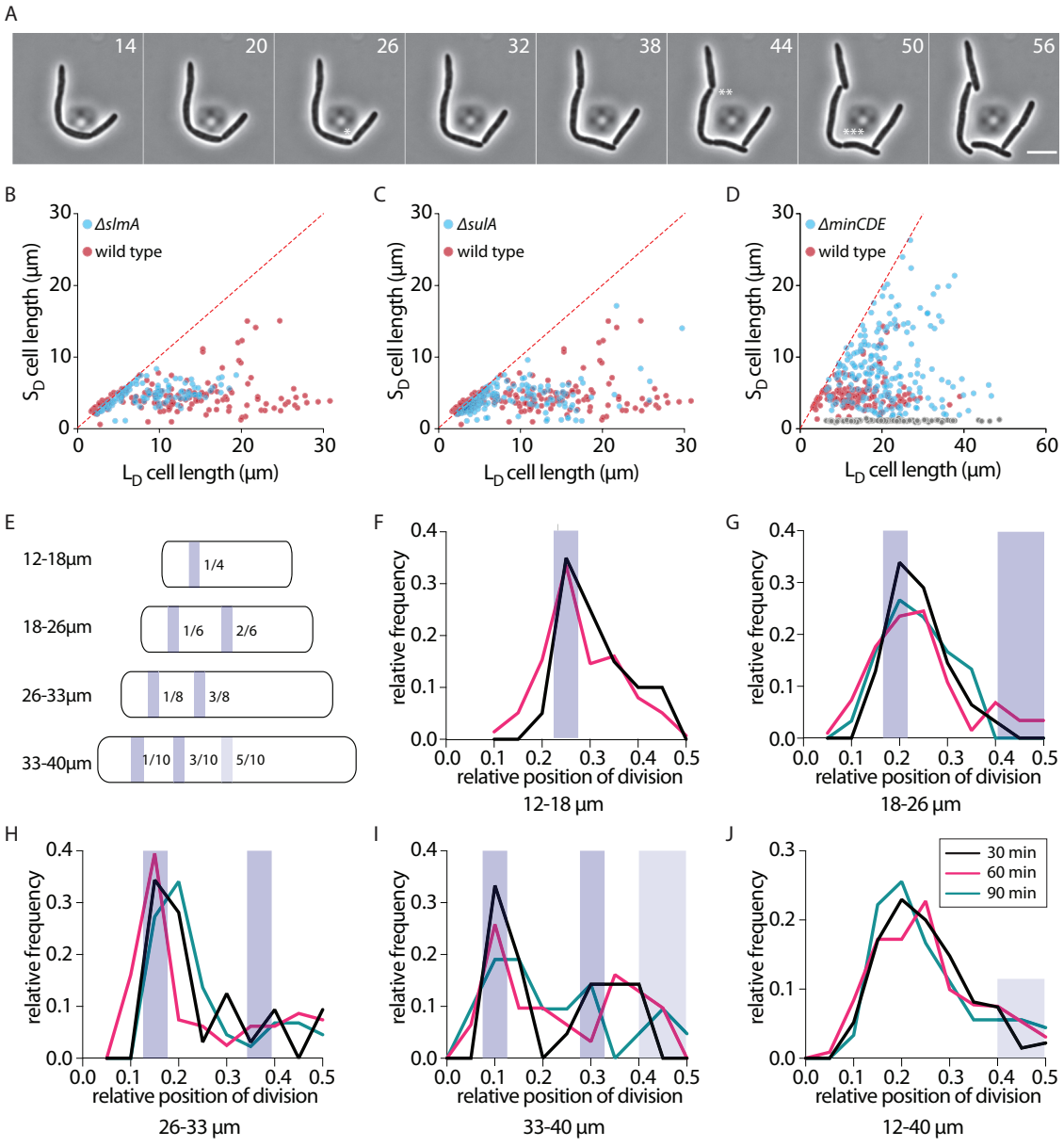

FIGURE 3: Role of Min-system in division positioning. (A) Representative time-lapse montage of division in wild-type cells during damage recovery. (B–D) Cell length of long daughter (L_D) and short daughter (S_D) generated from a DNA damage-induced filament during recovery for *slmA* ($n = 144$), *sulA* ($n = 246$), and *minCDE* ($n = 186$) backgrounds, respectively (blue dots; minicells are shown in gray). As a reference, lengths for wild type ($n = 137$) during recovery are shown in red. The red line plots the expected values if all cells were dividing at their midpoint. (E) Schematic representation of the Min-driven division site rule (figure adapted from Wehrens *et al.*, 2018). Location of division for various filament length bins is shown with the blue band. Precise location of division (relative to cell length) is depicted inside each cell. (F) Distribution of relative position of division for filaments between 12 and 18 μm for 30 or 60 min of damage treatment. Data are not shown for 90 min of treatment as the number of filaments in this length range in 90 min treatment is low. Location of division as determined by the Min-rule is shown as a shaded bar. (G–I) As F for filaments between 18 and 26, 26 and 33, and 33 and 40 μm, respectively. (J) As F for all filaments between 12 and 40 μm. Location of potential midcell division is shown with the shaded bar (n [all] = 135 [30 min], 453 [60 min], 95 [90 min]).

at the polar site in damage-induced filaments when compared with division-inhibited filaments (Wehrens *et al.*, 2018); it is possible that this is due to variability in additional factors, such as differences in growth rates. Our observations are largely consistent with previous studies, and suggest that Min is the primary driver of division location in damage-induced filaments as well. However, a significant fraction of divisions occur at the most polar sites and not at other sites predicted by the Min-rule.

Impact of chromosome and terminus segregation on division regulation

We wondered which additional factors could contribute to higher frequency of polar divisions in the case of damage-induced filaments. Given that chromosomes in DNA damage-induced filaments are no longer segregated (Odsbu and Skarstad, 2014; Vickridge *et al.*, 2017) but chromosome replication continues to proceed (Rudolph *et al.*, 2007; Lloyd and Rudolph, 2016), we asked whether

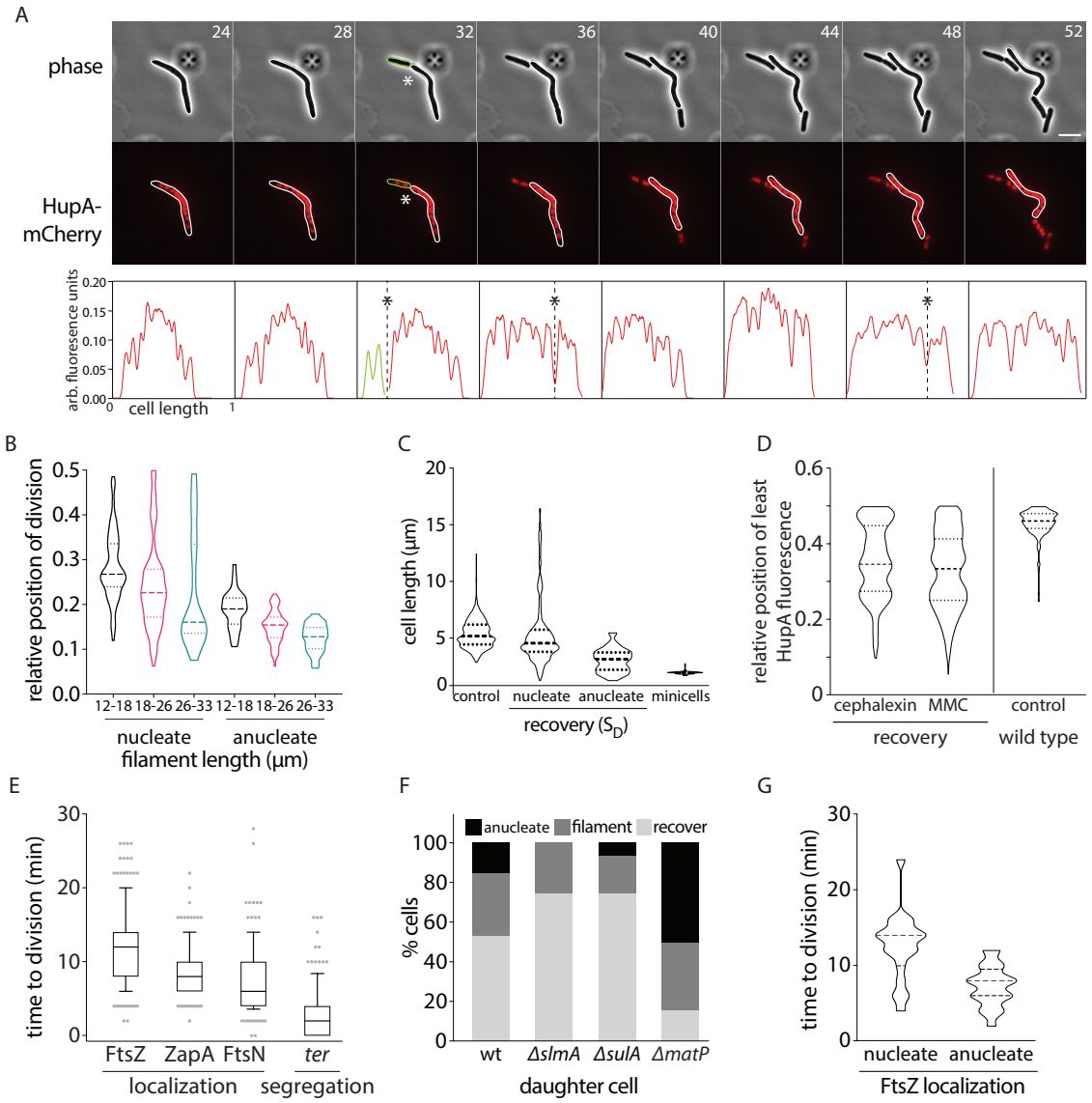

FIGURE 4: Impact of chromosome and terminus segregation on division regulation. (A) Representative time-lapse montage of division in cells during recovery. Gray: phase; red, HupA-mCherry (chromosome); scale bar = 5 μm; time in minutes. Fluorescence intensity traces for the cell in montage is provided below. Division sites are marked with "*". (B) Distribution of relative position of division for filaments between 12 and 18, 18 and 26, and 26 and 33 μm is plotted for nucleate and anucleate (from wild-type and *matP* backgrounds) divisions (n = 398 [nucleate] and 160 [anucleate]). (C) Cell length distribution for wild-type cells (no perturbation) is plotted. Along with this, cell length distribution of S_D during DNA damage recovery is plotted for nucleate cells and anucleate cells. To highlight the distinction between these cell division events and minicell formation, cell length distribution of minicells (from *min*-deleted cells) is also shown. (n = 1110 [control], 531 [nucleate S_D], 41 [anucleate S_D], 117 [minicells]). (D) Position of least intensity of HupA fluorescence (gaps between chromosomes) plotted as a function of cell length (from one pole to midcell) in recovering MMC or cephalexin-treated filaments. As reference, these data are also shown for wild-type cells with no damage treatment (control; n = 191 [cephalexin], 476 [MMC], 150 [control]). (E) Distribution of time to division after FtsZ, ZapA, and FtsN localization to division site is plotted. Along with this, time to division after segregation of *terminus* (*ter*) during recovery after MMC treatment is also shown (n = 103 [FtsZ], 102 [ZapA], 127 [FtsN], 123 [*ter*]). (F) Percentage of S_D that are anucleate, recover, and filament is plotted for wild type and deletions of *slmA*, *sulA*, and *matP*, during DNA damage recovery (n = 103 [wild type], 105 [*slmA*], 105 [*sulA*], 103 [*matP*]). (G) Time from FtsZ localization to division completion is plotted for divisions that result in nucleated or anucleated S_D cells (n = 231 [nucleate], 71 [anucleate]).

chromosome segregation dynamics in filaments could additionally contribute to control of division, thus influencing the division pattern observed. Hence, we followed chromosomes by imaging the nucleoid-associated protein, HupA (Marceau *et al.*, 2011; Youngren *et al.*, 2014), tagged with mCherry after mitomycin-C (MMC) or cephalexin treatment (Figure 4A).

When we tracked division in conjunction with chromosome dynamics, we observed that early divisions in filaments resulted in 15 ± 6% of daughter cells that were anucleated (Supplemental Figure S4A). These cells were smaller on average when compared with nucleated cells, but were distinct from minicells (Figure 4C). Anucleate divisions (38%) occurred at the first division event during

recovery and this percentage reduced to <7% by the third division. The production of anucleate cells early during division is consistent with Min being the primary driver of divisions, independent of chromosome segregation. When we plotted the relative position of division for anucleate cells, here too division tended to occur at the most polar site as predicted by the Min-rule (consistent with our observations above; Figure 4B). However, division position was less noisy in the case of anucleate division (and more precisely aligned with the Min-rule for the most polar division site) when compared with nucleated divisions. Indeed, anucleate daughter size distribution was also well described by the Min-driven rule for end-point division, with some noise (mean anucleate cell size was 3.4 ± 0.87 μm when compared with a mean cell size of 3.8 ± 0.59 μm as predicted by the Min-rule). However, the Min-rule alone seemed to be insufficient to describe the nucleated division events that had a broader division position and daughter size distribution (mean nucleate cell size was 5.4 ± 2.78 μm vs. 3.8 ± 0.59 μm as predicted by the Min-rule). While we are not sure why division occurs at a higher frequency at polar sites, we propose that this may be driven by the presence of chromosome-free regions closer to the cells poles (Figure 4D and Supplemental Figure S4A), and based on the following additional observations regarding the dynamics of chromosome (and specifically *terminus)* segregation:

1. Location of the FtsZ-ring correlated with where the chromosomes were most segregated at the time of division in damage-recovery conditions. Furthermore, chromosomes tended to be better segregated away from midcell (via estimation of location of the least intensity of HupA fluorescence, as a proxy for nucleoid-free regions; Figure 4D and Supplemental Figure S4, B and C).
2. The *terminus* region of the chromosome (tracked using the *parS*-ParB locus labeling system (Nielsen *et al.*, 2006; Espéli *et al.*, 2012) segregated just before or concomitant with division. While the bulk of the chromosome segregated well before division, and divisome components downstream from FtsZ (ZapA and FtsN) localized 8 min and 6 min before division, respectively, a single *terminus* focus could be observed to persist in the chromosome-free region, where constriction had begun to occur. Constriction was completed and division occurred just before or concomitant with the *termini* splitting into two foci on either side of the division plane, within 2 min on average (Figure 4E and Supplemental Figure S4, D and E).
3. Perturbing *terminus* localization and segregation negatively impacted recovery from DNA damage. Deletion of *matP*, a key player in modulating *terminus* dynamics specifically in nondamage conditions (Mercier *et al.*, 2008; Espéli *et al.*, 2012; Nolivos *et al.*, 2016; Lioy *et al.*, 2018), resulted in a significant increase in anucleate cell production, with 50 ± 3% of divisions being anucleated. This is in contrast to wild-type filaments or deletions of *slmA* or *sulA* that do not affect *terminus* segregation, but instead regulate divisome assembly (Figure 4F). Indeed, *matP*-deleted cells also showed a delay in recovery from DNA damage (as measured by colony-forming units) when compared with wild-type cells (Supplemental Figure S4F).
4. Based on these observations, we hypothesized that if chromosome segregation has no effect on division dynamics, then the time from divisome assembly to cell division should be the same between anucleated and nucleated divisions. However, if segregation had an effect, then the dynamics would vary between the two types of divisions. In the case of divisions that resulted in the production of anucleated cells, we found that the average period between FtsZ assembly at the division site to cell division was 7 min. In contrast, in the case of nucleated divisions, we noticed that FtsZ localized in the nucleoid-free regions for significantly longer, with an average of 12 min before division (Figure 4G). While the mechanistic details of this process warrants future investigation (see *Discussion*), these data are in support of a scenario where, in addition to Min-driven division site determination, chromosome (and specifically *terminus*) segregation contributes to the regulation of cell division in damage-induced filaments.

DISCUSSION

In laboratory conditions, wild-type *E. coli* maintains a distinct periodicity of cell growth and division that appears to be coupled with chromosome replication and segregation (Donachie, 1968; Hill *et al.*, 2012; Arjes *et al.*, 2014; Campos *et al.*, 2014; Kleckner *et al.*, 2014; Taheri-Araghi *et al.*, 2015; Wallden *et al.*, 2016; Micali *et al.*, 2018). However, it is becoming increasingly evident that bacteria can exist in diverse morphological states, in part dictated by their environmental conditions (Justice *et al.*, 2008; Jonas, 2014; Kysela *et al.*, 2016; Yang *et al.*, 2016; Caccamo and Brun, 2018; MacCready and Vecchiarelli, 2018; Muraleedharan *et al.*, 2018; Heinrich *et al.*, 2019). Even *E. coli* can become highly filamentous under conditions of stress such as during infection (Justice *et al.*, 2004; Horvath *et al.*, 2011). Transitions into filamentous morphologies are thought to confer several advantages such as avoiding phagocytosis via the host immune response or providing a means to dilute the effects of any inhibitors present in the surroundings (Justice *et al.*, 2004, 2008; Horvath *et al.*, 2011; Yang *et al.*, 2016). Recent reports have also suggested that filamentation (at least in the case of *E. coli* treated with ciprofloxacin) may be the first step toward the emergence of antibiotic resistance as daughter cells carry mutations making them ciprofloxacin resistant (Bos *et al.*, 2015). Thus, it becomes important to understand how bacterial cells enter and exit these filamentous states to ensure survival under stress.

Here, we find that damage-induced filaments tend to divide asymmetrically, with a high frequency of such divisions resulting in the production of short daughter cells of wild-type size. While the filament itself may or may not recover to wild-type size and still retains damaged DNA, most short daughters generated from a single filament can go on to replicate and divide as wild-type cells. The concept of asymmetric partitioning of cellular components during stress seems to have been coopted by several bacterial systems (Schramm *et al.*, 2019) including *Mycobacterium tuberculosis,* where one daughter cell inherits the growing pole, while the other has to assemble a growth pole de novo. This results in difference in susceptibility to antibiotic treatment between the two cell types; the daughter cell with the growing pole is more sensitive to cell wall synthesis inhibitors when compared with cells that inherited the nongrowing pole (Aakre and Laub, 2012; Aldridge *et al.*, 2012). The swarmer cells of *Proteus mirabilis* and *Vibrio parahaemolyticus* (MacCready and Vecchiarelli, 2018; Muraleedharan *et al.*, 2018) use the Min-system to regulate asymmetric cell division to allow for such division while still preserving the population of filamentous cells. Dim-light stress induces filamentation in the photosynthetic cyanobacterium *Synechococcus elongatus*, which then divides asymmetrically via positioning by the Min-system (Liao and Rust, 2018). Even in *E. coli* filaments generated in non-DNA damage conditions, studies have reported poleward division events (Adler and Hardigree, 1965; Begg and Doanachie, 1977; Taschner *et al.*, 1988; Mileykovskaya *et al.*, 1998; Wehrens *et al.*, 2018). It is possible that asymmetric division in damage-induced filaments confers such advantages to short daughters (inheritance of damage-free chromosomes or

possible ability of short daughters to swarm away from the stress condition). Taken together, this suggests that switching from midcell to filamentation-based division may be a universal method for cells under stress to ensure viable cell divisions.

How is S_D size determined in damage-induced filament divisions? Previous studies have suggested a central role for the Min-system in determining division site rules in filamentous *E. coli* (Begg and Doanachie, 1977; Taschner *et al.*, 1988; Wehrens *et al.*, 2018). Our observations in *min*-deleted cells are consistent with the same. However, we observe that midcell divisions may be suppressed at certain filament lengths where such division should be permitted as predicted by the Min-rule seen in division-inhibited filaments (Wehrens *et al.*, 2018). Indeed, division position is more noisy (less accurate) in the case of damage-induced filaments; it is possible that this is due to variability in additional factors in the case of damage-induced filaments, such as differences in growth rates or chromosome segregation dynamics.

We propose the following scenario with regards to polar divisions in damage-induced filaments, based on our results and in line with previous studies: The MinCDE system is the primary contributor to determining the location of divisome assembly. However, time taken to complete division is additionally regulated by chromosome segregation. For example, the disorganized nature of damaged chromosomes, thought to facilitate recombination-based repair (Odsbu and Skarstad, 2014; Vickridge *et al.*, 2017), can add a layer of regulation with chromosome segregation imposing a delay in division completion. The increased frequency of polar division could be a consequence of better chromosome segregation toward cell poles, where chromosome-free spaces are available as a result of molecular crowding (Wu *et al.*, 2019). In most cases cell growth occurs between divisions—it could be that division delay lasts until the Min "division point" and the completion of chromosome "segregation" become aligned. However, in some cases we also observe consecutive divisions without the addition of length in between.

It is currently unclear as to whether and how these two processes (Min-driven division site placement and completion of chromosome segregation) are mechanistically connected. Alternately, it is also possible that divisome positioning and completion of chromosome segregation are concurrent processes that are not molecularly coupled. Indeed, the production of anucleate cells early during filament division as well as when *terminus* segregation is perturbed are consistent with the idea that segregation is not necessary for cell division, with the Min-system likely being the dominant driver of division (Wehrens *et al.*, 2018). In the case of nucleated divisions, additional mechanisms may contribute to the regulation of division completion, possibly to ensure the completion of chromosome replication and segregation before division, in order to avoid deleterious effects of DNA guillotining (Hendricks *et al.*, 2000). For example, Rudolph *et al.* (2007) found that cells treated with UV damage continued to initiate new rounds of replication but did not complete the same, likely due to the presence of lesions blocking replication progression. Thus, they observed fewer *terminus* copies when compared with the *origin*. The following observations led us to speculate the possibility of such a division checkpoint being regulated by the *terminus* region of the chromosome during damage recovery (affecting time taken to complete division): 1) In the absence of chromosome segregation, anucleate cells are produced (as also reported by Mulder and Woldringh, 1989). These divisions are faster than nucleated divisions, suggesting that chromosome segregation can impose a delay on timing of division completion. 2) The *terminus* region of the chromosome persists in nucleoid gaps and segregates just before or concomitant with division. 3) Perturbing *terminus* organization and segregation via deletion of *matP* has an impact on outcomes of nucleated cell division and recovery after damage.

The mechanistic basis of such division regulation warrants future investigations. The system characterized in this study provides the ability to assess these rate-limiting steps of division (such as completion of replication) and further probe the mechanisms of asymmetric chromosome segregation that preferentially results in the production of daughter cells devoid of damage. For example, MatP has two independent functions of *ter* region organization and *ter* anchoring with the divisome (Bailey *et al.*, 2014; Männik *et al.*, 2016; Nolivos *et al.*, 2016). It would be important to understand which of these activities is specifically necessary in the recovery process. The idea that the *terminus* region of the chromosome can significantly influence division outcomes has been investigated by several studies in the context of nondamaged *E. coli* cells (Männik and Bailey, 2015). For example, earlier studies have suggested that perturbing chromosome dimer resolution (via *dif* mutants) can result in DNA guillotining and subsequent blockage in cell division due to damaged DNA. Such a checkpoint also results in an increase in the production of anucleate cells from filaments (Hendricks *et al.*, 2000). In steady-state conditions, mechanisms including nucleoid occlusion, Min-system, and *terminus* linkage help coordinate cell division with chromosome segregation to prevent such guillotining (Männik and Bailey, 2015). The *ter* linkage (via MatP-divisome interactions) also influences Z-ring positioning by acting as a landmark for divisome assembly, thus ensuring precise positioning of the divisome. Lack of this anchoring perturbs division accuracy in steady-state conditions (Espéli *et al.*, 2012; Bailey *et al.*, 2014). In addition to regulating divisome positioning, Buss *et al.* found that the MatP-FtsZ linkage also slowed down constriction rates, likely contributing to coordination of chromosome segregation with cell division in steady-state conditions (Buss *et al.*, 2015). Thus, our observations with regard to *terminus* dynamics and MatP-associated phenotypes lend support to the likely importance of this linkage in division control and a possible role for concurrency (Micali *et al.*, 2018) between two mechanisms of division regulation for division accuracy in damage-induced filaments as well. The conservation of asymmetric division in a range of stress-induced bacterial filaments underscores the contribution of this process in facilitating robust exit from the DNA damage checkpoint via the generation of fit, damage-free daughter cells.

MATERIALS AND METHODS

Bacterial strains and growth conditions

Strains and plasmids used in the study are listed in Supplemental Table S1. Oligos used to verify deletions via PCR are listed in Supplemental Table S2. Transductions were conducted with P1 phage following the protocol in Thomason *et al.* (2007). Transformations were performed following standard chemical competence protocols for *E. coli*. Cells were grown at 37°C in either rich media (LB: for 1 L dissolved 10 g tryptone, 5 g yeast extract, and 10 g NaCl in double-distilled water) or minimal media (M9-Cas: for 1 L dissolved 5 g glucose, 1 g casamino acids, 1 ml of 0.5% thiamine, 1 ml of 1M $MgSO_4$, and 200 ml 5× M9 salts in double-distilled water). DNA damage was induced with 1 μg/ml MMC for 30, 60, or 90 min (LB) or 90 min (M9-Cas; unless otherwise indicated). Cell division was inhibited using 5 μg/ml cephalexin for 60 min (LB) or 90 min (M9-Cas).

Fluorescence microscopy

Imaging was performed on a wide-field, epifluorescence microscope (Nikon Eclipse Ti-2E, with motorized xy-stage, Z-drift correction), 63X plan apochromat objective (NA 1.41), pE4000 light source

(CoolLED), OkoLab incubation chamber, and Hamamatsu Orca Flash 4.0 camera. Images were acquired using the NIS-elements software (version 5.1). Microfluidics imaging was performed using the CellASIC-ONIX2 microfluidic system, temperature controlled CellASIC-ONIX2 Manifold XT, and CellASIC ONIX plate for bacteria cells (B4A; Merck). Details of the imaging and acquisition setting are described here (Raghunathan and Badrinarayanan, 2019).

Time-course and time-lapse imaging

Details of independent repeats of experiments: for damage-recovery (60 min) experiments (with *hupA-mCherry*), seven biological replicates were performed. Δs*lmA* experiments were performed twice (biological replicates). FtsZ-GFP/ZapA-GFP recovery time-lapse imaging was conducted independently six times. Wild-type (no damage) time-lapse experiments were performed four times independently. Three independent replicates were performed for all other experiments reported in this study.

For the recovery time course, cells were grown overnight in LB or M9-Cas, back diluted to OD_{600} = ~0.01 and allowed to grow to OD_{600} = ~0.1. Culture was then treated with MMC or cephalexin for 60 min (LB) or 90 min (M9-Cas). Cells were pelleted, washed with fresh media, resuspended to OD_{600} = ~0.1, and then allowed to recover from damage treatment. Cultures were maintained in log phase (OD_{600} = ~0.1–0.4) throughout the experiment. For time course, samples for microscopy were collected at the time points indicated. Culture (1 ml) was pelleted, resuspended in 100 µl, and then spotted on a 1% agarose pad and imaged (Chimthanawala and Badrinarayanan, 2019).

For time-lapse experiments, damaged-induced cells were pelleted and washed with fresh media and were either loaded into the microfluidics device or spotted on a 1.5% agarose pad (made with appropriate growth media) and imaged. All time-lapse images were taken every 30 s or 2 min for ~3 h. For the FtsN imaging experiments, cells were induced with 0.1% rhamnose for 1 h before imaging. For MinD-GFP imaging, cells were induced with 0.2 mM IPTG for 90 min before imaging. Inducers were maintained in the agarose pads or microfluidic plates. Experiments were performed in LB unless otherwise indicated.

RNA sequencing

Protocol for RNA extraction described in Badrinarayanan *et al*. (2017) was followed. Briefly, cell pellets were collected during the recovery time course at the indicated times. RNA was extracted using the Direct-zol RNA MiniPrep (Zymo, Cat. no. R2052A81) and RNA Clean & Concentrator-25 (Zymo, Cat. no. R1018A82). RNA libraries were prepared using the TruSeq Stranded mRNA Library Preparation kit at NCBS next generation sequencing facility. Libraries were sequenced using the Illumina MiSeq sequencing platform. Raw reads (single end; read length = 50 base pairs) were obtained as .fastq files. The reference genome sequence (.fna) and annotation (.gff) files for the same strain (accession number: NC_000913.3) were downloaded from the National Centre for Biotechnology Information ftp website ("ftp.ncbi.nlm.nih.gov"). The raw read quality was checked using the FastQC software (version v0.11.5). BWA (version 0.7.12-r1039; Li and Durbin, 2009; Burroughs and Aravind, 2016) was used to index the reference genome. Reads with raw read quality ≥20 were aligned using the BWA aln -q option. SAMTOOLS (version 0.1.19-96b5f2294a; Li *et al*., 2009) was used to filter out the multiply mapped reads. BEDTOOLS (version 2.25.0; Quinlan and Hall, 2010) was used to calculate the reads count per gene using the annotation file (.bed) in a strand-specific manner. Normalized counts were obtained using trimmed mean of M values normalization of EdgeR package. The counts across time were calculated relative to the no damage control. The log_2-fold change in expression was plotted from this. Raw data can be accessed via EBI ArrayExpress (EMTAB9696).

Image analysis

Images acquired were visualized and processed using ImageJ (Schindelin *et al*., 2012, 2015). Data were pooled from two to six replicates per experiment and segmentation was performed using Oufti (Paintdakhi *et al*., 2016). Foci tracking was accomplished using the Spotfinder Z function of MicrobeTracker (Sliusarenko *et al*., 2011). For recovery time course, custom MATLAB scripts were used to extract cell length and total fluorescence intensity information for each cell. Anucleate cells were identified using a threshold of 0.02 a.u. for total intensity of HupA-GFP in the cells. For time-lapse analysis, at each division, the longer cell was termed L_D and the smaller cell given the identity of S_D. A custom MATLAB script was used to the extract the lengths of the L_D and S_D at each division, the length added between divisions and time between divisions. Daughter cells were classified as "recovers" if at their first division, their length was <10 µm and they divided symmetrically. Cells that were longer at their first division and divided asymmetrically were classified as "filaments." RecA foci numbers were obtained using Spotfinder Z and combined with cell length information from Oufti. The number of FtsZ rings in a cell were obtained using Spotfinder Z and combined with cell length information from Oufti. For analysis of constrictions and divisions, we used Oufti, which allows subpixel segmentation of phase contrast images of cells in a time-lapse. The method is illustrated in Figure 2 and Supplemental Figure S2. In Figure 2G, a phase profile for a wild-type cell before and after division is plotted. While the profile is, on average, a flat line for most of the time imaged, one can identify a constriction before division (marked with *). Similarly in Figure 2H, the phase profile for a filamentous cell (DNA damage-induced) undergoing division is plotted. If the phase profile deviates by 20–25% of the cell width, it is called a constriction. If the phase profile is discontinuous (with a gap), then it is marked as a division by the segmentation algorithm automatically. For nucleoid tracking, fluorescence intensity profiles of HupA-mCherry, obtained from Oufti, was used. Data was first smoothened using a Savitzgy-Golay filter (Luo *et al*., 2005). Following this the fluorescence profile was inverted so that the regions of lowest fluorescence now had the highest values. Peaks were determined using the peak prominence function after setting a threshold of half the maximum intensity for each frame. Peaks correspond to lowest fluorescence intensity in the cell. Regions right next to the cell poles were excluded. This information was combined with FtsZ foci tracked using Spotfinder Z to obtain relative positions of the lowest fluorescence intensity in the cell and FtsZ-ring. The formation of FtsZ, ZapA, and FtsN foci, and segregation of the single *terminus* focus (ParB-GFP) to two foci at the site of division, were scored manually along with time to division.

ACKNOWLEDGMENTS

The authors are grateful to Thomas Bernhardt, Steven Sandler, Suckjoon Jun, Bill Soederstroem, Fred Boccard, Olivier Espeli, Christian Lesterlin, Ramanujam Srinivasan, and Manjula Reddy for generous sharing of strains and plasmids. The authors acknowledge assistance from Ismath Sadhir in RNA extraction; Nitish Malhotra in RNA-seq analysis; Aditya Jalin, Alex Sam Thomas, and Aalok Varma in writing MATLAB scripts; as well as the Central Imaging and Flow Facility and Next-Generation Genomics Facility. The authors thank anonymous referees, Fagwei Si, Piet de Boer, Raj Ladher, Michael

Laub, Tung Le, and members of the A.B. lab for helpful discussions and feedback on the manuscript. This work is supported by funding from National Centre For Biological Sciences–Tata Institute of Fundamental Research (Department of Atomic Energy, Government of India, under project no. 12-R&D-TFR-5.04-0800; A.B. and S.K.), by an Human Frontier Space Program Career Development award (A.B.), and funding from the Simons Foundation (S.K.).

REFERENCES

Aakre CD, Laub MT (2012). Asymmetric cell division: a persistent issue? Dev Cell. 22, 235–236.

Adler HI, Hardigree AA (1965). Growth and division of filamentous forms of *Escherichia coli*. J Bacteriol 90, 223–226.

Aldridge BB, Fernandez-Suarez M, Heller D, Ambravaneswaran V, Irimia D, Toner M, Fortune SM (2012). Asymmetry and aging of mycobacterial cells lead to variable growth and antibiotic susceptibility. Science 335, 100–104.

Arjes HA, Kriel A, Sorto NA, Shaw JT, Wang JD, Levin PA (2014). Failsafe mechanisms couple division and DNA replication in bacteria. Curr Biol 24, 2149–2155.

Badrinarayanan A, Le TBK, Spille J-H, Cisse II, Laub MT (2017). Global analysis of double-strand break processing reveals in vivo properties of the helicase-nuclease complex AddAB. PLoS Genet 13, e1006783.

Bailey MW, Bisicchia P, Warren BT, Sherratt DJ, Männik J (2014). Evidence for divisome localization mechanisms independent of the Min system and SlmA in *Escherichia coli*. PLOS Genet 10, e1004504.

Begg KJ, Doanachie WD (1977). Growth of the *Escherichia coli* cell surface. J Bacteriol 129, 1524–1536.

Bernhardt TG, de Boer PAJ (2005). SlmA, a nucleoid-associated, FtsZ binding protein required for blocking septal ring assembly over chromosomes in *E. coli*. Mol Cell 18, 555–564.

Bos J, Zhang Q, Vyawahare S, Rogers E, Rosenberg SM, Austin RH (2015). Emergence of antibiotic resistance from multinucleated bacterial filaments. Proc Natl Acad Sci USA 112, 178–183.

Burroughs AM, Aravind L (2016). RNA damage in biological conflicts and the diversity of responding RNA repair systems. Nucleic Acids Res 44, 8525–8555.

Buss J, Coltharp C, Shtengel G, Yang X, Hess H, Xiao J (2015). A multilayered protein network stabilizes the *Escherichia coli* FtsZ-ring and modulates constriction dynamics. PLOS Genet 11, e1005128.

Caccamo PD, Brun YV (2018). The molecular basis of noncanonical bacterial morphology. Trends Microbiol 26, 191–208.

Campos M, Surovtsev IV, Kato S, Paintdakhi A, Beltran B, Ebmeier SE, Jacobs-Wagner C (2014). A constant size extension drives bacterial cell size homeostasis. Cell 159, 1433–1446.

Chandler-Brown D, Schmoller KM, Winetraub Y, Skotheim JM (2017). The adder phenomenon emerges from independent control of pre- and post-start phases of the budding yeast cell cycle. Curr Biol 27, 2774–2783.e3.

Chimthanawala A, Badrinarayanan A (2019). Live-cell fluorescence imaging of RecN in *Caulobactercrescentus* under DNA damage. Methods Mol Biol 2004, 239–250.

Chung HS, Yao Z, Goehring NW, Kishony R, Beckwith J, Kahne D (2009). Rapid β-lactam-induced lysis requires successful assembly of the cell division machinery. Proc Natl Acad Sci 106, 21872–21877.

Dapa T, Fleurier S, Bredeche M-F, Matic I (2017). The SOS and RpoS regulons contribute to bacterial cell robustness to genotoxic stress by synergistically regulating DNA polymerase Pol II. Genetics 206, 1349–1360.

de Boer PAJ, Crossley RE, Rothfield LI (1989). A division inhibitor and a topological specificity factor coded for by the minicell locus determine proper placement of the division septum in *E. coli*. Cell 56, 641–649.

Dewachter L, Verstraeten N, Fauvart M, Michiels J (2018). An integrative view of cell cycle control in *Escherichia coli*. FEMS Microbiol Rev 42, 116–136.

Donachie WD (1968). Relationship between cell size and time of initiation of DNA replication. Nature 219, 1077–1079.

Espéli O, Borne R, Dupaigne P, Thiel A, Gigant E, Mercier R, Boccard F (2012). A MatP–divisome interaction coordinates chromosome segregation with cell division in *E. coli*. EMBO J 31, 3198–3211.

Galli E, Gerdes K (2012). FtsZ-ZapA-ZapB interactome of *Escherichia coli*. J. Bacteriol 194, 292–302.

Harris LK, Theriot JA (2016). Relative rates of surface and volume synthesis set bacterial cell size. Cell 165, 1479–1492.

Harris LK, Theriot JA (2018). Surface area to volume ratio: a natural variable for bacterial morphogenesis. Trends Microbiol 26, 815–832.

Heinrich K, Leslie DJ, Morlock M, Bertilsson S, Jonas K (2019). Molecular basis and ecological relevance of caulobacter cell filamentation in freshwater habitats. MBio 10, doi:10.1128/mBio.01557-19.

Hendricks EC, Szerlong H, Hill T, Kuempel P (2000). Cell division, guillotining of dimer chromosomes and SOS induction in resolution mutants (dif, xerC and xerD) of *Escherichia coli*. Mol Microbiol 36, 973–981.

Hill NS, Kadoya R, Chattoraj DK, Levin PA (2012). Cell size and the initiation of DNA replication in bacteria. PLoS Genet 8, e1002549.

Horvath DJ, Li B, Casper T, Partida-Sanchez S, Hunstad DA, Hultgren SJ, Justice SS (2011). Morphological plasticity promotes resistance to phagocyte killing of uropathogenic *Escherichia coli*. Microbes Infect 13, 426–437.

Jonas K (2014). To divide or not to divide: control of the bacterial cell cycle by environmental cues. Curr Opin Microbiol 18, 54–60.

Justice SS, Hung C, Theriot JA, Fletcher DA, Anderson GG, Footer MJ, Hultgren SJ (2004). Differentiation and developmental pathways of uropathogenic *Escherichia coli* in urinary tract pathogenesis. Proc Natl Acad Sci USA 101, 1333–1338.

Justice SS, Hunstad DA, Cegelski L, Hultgren SJ (2008). Morphological plasticity as a bacterial survival strategy. Nat Rev Microbiol 6, 162–168.

Kantor GJ, Deering RA (1966). Ultraviolet radiation studies of filamentous *Escherichia coli* B. J Bacteriol 92, 1062–1069.

Kleckner NE, Chatzi K, White MA, Fisher JK, Stouf M (2018). Coordination of growth, chromosome replication/segregation, and cell division in *E. coli*. Front Microbiol 9, 1469.

Kleckner N, Fisher JK, Stouf M, White MA, Bates D, Witz G (2014). The bacterial nucleoid: nature, dynamics and sister segregation. Curr Opin Microbiol 22, 127–137.

Kreuzer KN (2013). DNA damage responses in prokaryotes: regulating gene expression, modulating growth patterns, and manipulating replication forks. Cold Spring Harb Perspect Biol 5, a012674.

Kysela DT, Randich AM, Caccamo PD, Brun YV (2016). Diversity takes shape: understanding the mechanistic and adaptive basis of bacterial morphology. PLoS Biol 14, e1002565.

Lambert A, Vanhecke A, Archetti A, Holden S, Schaber F, Pincus Z, Laub MT, Goley E, Manley S (2018). Constriction rate modulation can drive cell size control and homeostasis in *C. crescentus*. iScience. 4, 180–189.

Lesterlin C, Ball G, Schermelleh L, Sherratt DJ (2014). RecA bundles mediate homology pairing between distant sisters during DNA break repair. Nature 506, 249–253.

Li H, Durbin R (2009). Fast and accurate short read alignment with Burrows-Wheeler transform. Bioinformatics 25, 1754–1760.

Li H, Handsaker B, Wysoker A, Fennell T, Ruan J, Homer N, Marth G, Abecasis G, Durbin R, 1000 Genome Project Data Processing Subgroup (2009). The sequence alignment/map format and SAMtools. Bioinformatics 25, 2078–2079.

Liao Y, Rust MJ (2018). The Min oscillator defines sites of asymmetric cell division in cyanobacteria during stress recovery. Cell Syst. 7, 471–481.e6.

Lioy VS, Cournac A, Marbouty M, Duigou S, Mozziconacci J, Espéli O, Boccard F, Koszul R (2018). Multiscale structuring of the *E. coli* chromosome by nucleoid-associated and condensin proteins. Cell 172, 771–783.e18.

Lloyd RG, Rudolph CJ (2016). 25 years on and no end in sight: a perspective on the role of RecG protein. Curr Genet 62, 827–840.

Luo J, Ying K, Bai J (2005). Savitzky-Golay smoothing and differentiation filter for even number data. Signal Process 85, 1429–1434.

MacCready JS, Vecchiarelli AG (2018). In long bacterial cells, the Min system can act off-center. Mol. Microbiol. 109, 268–272.

Männik J, Bailey MW (2015). Spatial coordination between chromosomes and cell division proteins in *Escherichia coli*. Front Microbiol. 6, 306.

Männik J, Castillo DE, Yang D, Siopsis G, Männik J (2016). The role of MatP, ZapA and ZapB in chromosomal organization and dynamics in *Escherichia coli*. Nucleic Acids Res 44, 1216–1226.

Marceau AH, Bahng S, Massoni SC, George NP, Sandler SJ, Marians KJ, Keck JL (2011). Structure of the SSB-DNA polymerase III interface and its role in DNA replication. EMBO J 30, 4236–4247.

Mercier R, Petit M-A, Schbath S, Robin S, El Karoui M, Boccard F, Espéli O (2008). The MatP/*matS* site-specific system organizes the terminus region of the *E. coli* chromosome into a macrodomain. Cell 135, 475–485.

Micali G, Grilli J, Osella M, Lagomarsino MC (2018). Concurrent processes set *E. coli* cell division. Sci Adv 4, eaau3324.

Mileykovskaya E, Sun Q, Margolin W, Dowhan W (1998). Localization and function of early cell division proteins in filamentous *Escherichia coli* cells lacking phosphatidylethanolamine. J. Bacteriol 180, 4252–4257.

Mo AH, Burkholder WF (2010). YneA, an SOS-induced inhibitor of cell division in *Bacillus subtilis*, is regulated posttranslationally and requires the transmembrane region for activity. J Bacteriol 192, 3159–3173.
Modell JW, Hopkins AC, Laub MT (2011). A DNA damage checkpoint in *Caulobacter crescentus* inhibits cell division through a direct interaction with FtsW. Genes Dev 25, 1328–1343.
Modell JW, Kambara TK, Perchuk BS, Laub MT (2014). A DNA damage-induced, SOS-independent checkpoint regulates cell division in *Caulobactercrescentus*. PLoS Biol 12, e1001977.
Mukherjee A, Cao C, Lutkenhaus J (1998). Inhibition of FtsZ polymerization by SulA, an inhibitor of septation in *Escherichia coli*. Proc Natl Acad Sci USA 95, 2885–2890.
Mulder E, Woldringh CL (1989). Actively replicating nucleoids influence positioning of division sites in *Escherichia coli* filaments forming cells lacking DNA. J Bacteriol 171, 4303–4314.
Muraleedharan S, Freitas C, Mann P, Glatter T, Ringgaard S (2018). A cell length-dependent transition in MinD-dynamics promotes a switch in division-site placement and preservation of proliferating elongated *Vibrio parahaemolyticus* swarmer cells. Mol. Microbiol 109, 365–384.
Nielsen HJ, Ottesen JR, Youngren B, Austin SJ, Hansen FG (2006). The *Escherichia coli* chromosome is organized with the left and right chromosome arms in separate cell halves: *E. coli* chromosome segregation. Mol Microbiol 62, 331–338.
Nolivos S, Upton AL, Badrinarayanan A, Müller J, Zawadzka K, Wiktor J, Gill A, Arciszewska L, Nicolas E, Sherratt D (2016). MatP regulates the coordinated action of topoisomerase IV and MukBEF in chromosome segregation. Nat Commun 7, 10466.
Odsbu I, Skarstad K (2014). DNA compaction in the early part of the SOS response is dependent on RecN and RecA. Microbiology 160, 872–882.
Paintdakhi A, Parry B, Campos M, Irnov I, Elf J, Surovtsev I, Jacobs-Wagner C (2016). Oufti: an integrated software package for high-accuracy, high-throughput quantitative microscopy analysis. Mol Microbiol 99, 767–777.
Quinlan AR, Hall IM (2010). BEDTools: a flexible suite of utilities for comparing genomic features. Bioinformatics 26, 841–842.
Raghunathan S, Badrinarayanan A (2019). Tracking bacterial chromosome dynamics with microfluidics-based live cell imaging. Methods Mol Biol 2004, 223–238.
Rajendram M, Zhang L, Reynolds BJ, Auer GK, Tuson HH, Ngo KV, Cox MM, Yethiraj A, Cui Q, Weibel DB (2015). Anionic phospholipids stabilize RecA filament bundles in *Escherichia coli*. Mol Cell 60, 374–384.
Reyes-Lamothe R, Sherratt DJ (2019). The bacterial cell cycle, chromosome inheritance and cell growth. Nat Rev Microbiol 17, 467–478.
Rolinson GN (1980). Effect of β-Lactam antibiotics on bacterial cell growth rate. Microbiology 120, 317–323.
Rudolph CJ, Upton AL, Briggs GS, Lloyd RG (2010). Is RecG a general guardian of the bacterial genome? DNA Repair (Amst) 9, 210–223.
Rudolph CJ, Upton AL, Harris L, Lloyd RG (2009). Pathological replication in cells lacking RecG DNA translocase. Mol Microbiol 73, 352–366.
Rudolph CJ, Upton AL, Lloyd RG (2007). Replication fork stalling and cell cycle arrest in UV-irradiated *Escherichia coli*. Genes Dev 21, 668–681.
Schindelin J, Arganda-Carreras I, Frise E, Kaynig V, Longair M, Pietzsch T, Preibisch S, Rueden C, Saalfeld S, Schmid B, *et al*. (2012). Fiji: an open-source platform for biological-image analysis. Nat. Methods 9, 676–682.
Schindelin J, Rueden CT, Hiner MC, Eliceiri KW (2015). The ImageJ ecosystem: an open platform for biomedical image analysis. Mol Reprod Dev 82, 518–529.
Schramm FD, Schroeder K, Alvelid J, Testa I, Jonas K (2019). Growth-driven displacement of protein aggregates along the cell length ensures partitioning to both daughter cells in *Caulobacter crescentus*. Mol Microbiol 111, 1430–1448.
Si F, Le Treut G, Sauls JT, Vadia S, Levin PA, Jun S (2019). Mechanistic origin of cell-size control and homeostasis in bacteria. Curr Biol 29, 1760–1770.e7.
Sliusarenko O, Heinritz J, Emonet T, Jacobs-Wagner C (2011). High-throughput, subpixel precision analysis of bacterial morphogenesis and intracellular spatio-temporal dynamics. Mol Microbiol 80, 612–627.
Soifer I, Robert L, Amir A (2016). Single-cell analysis of growth in budding yeast and bacteria reveals a common size regulation strategy. Curr Biol 26, 356–361.
Suzuki H, Pangborn J, Kilgore WW (1967). Filamentous cells of *Escherichia coli* formed in the presence of mitomycin. J Bacteriol 93, 683–688.
Taheri-Araghi S, Bradde S, Sauls JT, Hill NS, Levin PA, Paulsson J, Vergassola M, Jun S (2015). Cell-size control and homeostasis in bacteria. Curr Biol 25, 385–391.
Taschner PE, Huls PG, Pas E, Woldringh CL (1988). Division behavior and shape changes in isogenic ftsZ, ftsQ, ftsA, pbpB, and ftsE cell division mutants of *Escherichia coli* during temperature shift experiments. J Bacteriol 170, 1533–1540.
Thomason LC, Costantino N, Court DL (2007). *E. coli* genome manipulation by P1 transduction. Curr Protoc Mol Biol Chapter 1:Unit 1.17. doi:10.1002/0471142727.mb0117s79.
Tonthat NK, Arold ST, Pickering BF, Van Dyke MW, Liang S, Lu Y, Beuria TK, Margolin W, Schumacher MA (2011). Molecular mechanism by which the nucleoid occlusion factor, SlmA, keeps cytokinesis in check. EMBO J 30, 154–164.
Tsang M-J, Bernhardt TG (2015). Guiding divisome assembly and controlling its activity. Curr Opin Microbiol 24, 60–65.
Vickridge E, Planchenault C, Cockram C, Junceda IG, Espéli O (2017). Management of *E. coli* sister chromatid cohesion in response to genotoxic stress. Nat. Commun 8, 14618.
Wallden M, Fange D, Lundius EG, Baltekin Ö, Elf J (2016). The synchronization of replication and division cycles in individual *E. coli* cells. Cell 166, 729–739.
Wehrens M, Ershov D, Rozendaal R, Walker N, Schultz D, Kishony R, Levin PA, Tans SJ (2018). Size laws and division ring dynamics in filamentous *Escherichia coli* cells. Curr Biol 28, 972–979.e5.
Wu F, Swain P, Kuijpers L, Zheng X, Felter K, Guurink M, Solari J, Jun S, Shimizu TS, Chaudhuri D, *et al*. (2019). Cell boundary confinement sets the size and position of the *E. coli* chromosome. Curr Biol 29, 2131–2144.e4.
Yang DC, Blair KM, Salama NR (2016). Staying in shape: the impact of cell shape on bacterial survival in diverse environments. Microbiol Mol Biol Rev 80, 187–203.
Youngren B, Nielsen HJ, Jun S, Austin S (2014). The multifork *Escherichia coli* chromosome is a self-duplicating and self-segregating thermodynamic ring polymer. Genes Dev 28, 71–84.